

Finite quark-mass effects in the NNLOPS POWHEG+MiNLO Higgs generator

Keith Hamilton,^a Paolo Nason,^b Giulia Zanderighi^{1c}

^a*Department of Physics and Astronomy, University College London,
London, WC1E 6BT, UK*

^b*INFN, Sezione di Milano Bicocca, Piazza della Scienza 3, 20126 Milan, Italy*

^c*Theory Division, CERN, CH-1211, Geneva 23, Switzerland*

E-mail: keith.hamilton@ucl.ac.uk, paolo.nason@mib.infn.it,
giulia.zanderighi@cern.ch

ABSTRACT: We include finite top- and bottom-mass effects in the next-to-next-to-leading order parton shower (NNLOPS) event generator for inclusive Higgs boson production in gluon fusion based upon the POWHEG+MiNLO approach. Since fixed-order results for quark-mass effects only reach NLO accuracy, we add them to the NNLOPS generator at that accuracy. We explore uncertainties related to the unknown all-order logarithmic structure of bottom-mass effects by comparing the assumption of full exponentiation to no exponentiation at all. Phenomenological results showing the effects of finite quark-masses in the NNLOPS simulation are presented. These suggest that the aforementioned uncertainty is well contained within the envelope of plain renormalization and factorization scale uncertainties.

KEYWORDS: QCD, Higgs Physics, Monte Carlo, LHC

¹On leave from Rudolf Peierls Centre for Theoretical Physics, University of Oxford, 1 Keble Road, UK

Contents

1	Introduction	1
2	Method	3
2.1	Mass effects in the HJ generator	3
2.2	Mass effects in the MiNLO procedure.	4
2.3	Quark-mass effects in HNNLO	6
3	Numerical study	6
3.1	The choice for the bottom mass.	6
3.2	Mass effects in matrix elements	7
3.3	Resummed mass effects	9
3.4	NNLOPS results	9
4	Conclusions	12
A	Technical details about b-mass effects in the MiNLO Sudakov	12
A.1	Phase space	13
A.2	Approximate matrix elements in the MiNLO Sudakov	16
A.2.1	Preliminaries	17
A.2.2	$qg \rightarrow Hq$ and $gq \rightarrow Hq$ approximate matrix elements	18
A.2.3	$gg \rightarrow Hg$ approximate matrix element	19

1 Introduction

Since the 2012 LHC discovery of a new spin-zero particle [1, 2], all subsequent experimental analysis (see e.g. [3–11]) has revealed that its properties are very much consistent with those predicted for the Standard Model (SM) Higgs boson. The discovery of what appears to be the SM Higgs boson, without any new physics below the TeV scale to stabilize its mass, poses profound and challenging questions for the theoretical community. By the same token, LHC studies to quantify the level of agreement between SM Higgs boson predictions and experimental measurements, by increasing the precision in both, has further intensified.

Thus far, tests and measurements of Higgs boson properties, in almost all cases, have focused on rather inclusive observables, such as production cross sections and branching ratios. However, even for fully inclusive quantities experimental analysis do often classify events in categories depending on the number of accompanying jets, and, at times, jet-vetos are used to enhance the signal-to-background ratio. In general these measurements require the use of fully exclusive Monte Carlo generators, possibly in combination with dedicated, theoretical calculations.

For gluon-fusion Higgs production, first differential measurements have been published in the second half of 2014 by the ATLAS collaboration [12, 13]. These measurements are at present statistically limited, however, forthcoming LHC Run-II data will lead to substantial improvements, and by the end of Run-II the measurement uncertainties are estimated to be substantially reduced. Full exploitation of these data, in particular the degree to which we are able to resolve or exclude new physics in the Higgs sector, requires that all theoretical tools, including Monte Carlo simulations, be as precise as possible.

Next-to-leading order calculations matched to parton showers (NLOPS) [14–16] are now the standard for fully exclusive Monte Carlo predictions and are indispensable tools for the LHC experimental collaborations.

Recently, NNLOPS generators for Higgs [17, 18] and Drell Yan [19, 20] production have also appeared. In particular, the generator of ref.[17], based upon the MiNLO method [21], is particularly attractive since it achieves NNLO accuracy without recourse to an unphysical partitioning of phase space. This generator is based upon the large m_t approximation of the Higgs coupling to gluons. On the other hand, it is known that finite quark-mass effects are important especially in the case of production in association to energetic jets, since the radiation resolves the internal structure of the gluon-Higgs effective coupling.

Finite quark-mass effects to the total cross section are known exactly at NLO ($\mathcal{O}(\alpha_s^3)$) in QCD perturbation theory [22–27]. Finite quark-mass effects on high transverse momentum Higgs production were first calculated at LO ($\mathcal{O}(\alpha_s^3)$) in refs. [28, 29] and, as an expansion in $1/m_t$, at NLO for finite top-quark-mass effects by Harlander et al. [30]. Some of the former finite quark-mass corrections have been implemented in public fixed order computer codes e.g. MCFM [31] FehiPro [32, 33] and SusHi [34].

Finite quark-mass effects have been included in NLOPS Monte Carlo simulations of Higgs boson production in POWHEG [35] and MC@NLO version 4.08 onwards [14]. Recently the Sherpa collaboration have introduced a treatment of finite top-mass effects [36] in the context of their multi-jet NLOPS merging scheme MEPS@NLO. Differences between the predictions of the POWHEG program of ref. [35] and MC@NLO, in particular regarding their response to the inclusion of finite b -quark-mass effects, have been a source of discussion and have stimulated further analytic work on the treatment of bottom-mass effects in resummed calculations.

The earliest analytic resummation work to include mass effects was that of Mantler and Wiesemann at LO+NLL accuracy [37], work which was later extended to include also MSSM effects [38]. An NNLL+NNLO resummation of the transverse momentum spectrum of the boson in the large- m_t limit was subsequently augmented with finite t - and b -quark-mass effects at the NLL+NLO level by Grazzini and Sargsyan [39]. Shortly following this work Banfi et al. presented an extension of their NNLL+NNLO large- m_t computation of the efficiency for Higgs boson production in the presence of a jet veto in ref. [40]. All of these analytic resummation computations took a different approach to the inclusion of finite b -quark-mass effects, in particular, to their handling of the enhanced $\sim \frac{1}{p_T^2} \frac{m_b^2}{m_H^2} \log^2 \frac{m_b^2}{p_T^2}$ terms in the region $m_b < p_T < m_H$.

In this work we address the extension of the NNLOPS event generator for Higgs boson

production in ref. [17] to include finite top- and bottom-quark-mass effects. In section two we present our theoretical rationale and method for doing this, with each subsection describing the implementation of finite quark-mass effects in a different layer of the event generator. Sec. 2.1 concerns the required modifications at the level of the underlying HJ NLOPS generator [41]. Sec. 2.2 enters into the discussion on the role of finite quark-mass effects and resummation, describing their implementation (or not) in the MiNLO Sudakov form factor and the theoretical justification for our approach. Sec. 2.3 describes how the finite quark-mass effects are accounted for in the NNLO predictions required for the reweighting stage. In Sec. 3 we present a selection of numerical results obtained with the new NNLOPS generator using various options to explore theoretical uncertainties. Conclusions are drawn in Sec. 4. Some technical details relevant to our new implementations are illustrated in the Appendix.

2 Method

In ref. [17] a generator that is NNLO accurate and includes parton shower effects (NNLOPS accurate from now on) was presented for inclusive Higgs production. This generator is based on the large m_t effective theory, in which the Higgs boson emitted from a top-loop is approximated by an effective tree-level coupling of the Higgs to gluons and the interaction of the Higgs boson to lighter quarks (including the bottom quark) is neglected.

Our goal here is to correct this NNLOPS Higgs generator in such a way that at least the most important mass effects are included. The NNLOPS generator relies upon three main components:

- the POWHEG HJ generator of ref. [41];
- the MiNLO procedure on HJ discussed in ref. [21];
- the NNLO fixed order calculation of ref. [39];
- the reweighting procedure described in ref. [17].

In the following we describe how, and to what extent, we include mass effects in the first three items of this list. The reweighting procedure remains obviously the same.

2.1 Mass effects in the HJ generator

An NLO calculation (i.e. of order α_s^4) of Higgs plus jet production including the finite quark-mass effects is not available at the moment, and we will thus resort to the following approximations. We begin by considering the quark-mass corrections due to the top loop only. We multiply all components (Born, virtual and real) of the infinite top mass approximation formulae by the ratio of the matrix elements for the production of a Higgs boson in association with a light parton, including exact one loop top mass dependence, divided by the same matrix element in the infinite top mass approximation. These matrix elements are all evaluated at the Born kinematics for the Born and virtual contribution, and at the

underlying Born kinematics for the real one.¹ This procedure guarantees that at the Born level the cross section has the full top mass dependence. The real emission cross section in the soft and collinear limits, has also fully corrected top mass dependence, and the same holds for the part of the virtual corrections that arises from virtual gluons of energy much below the top mass. Thus, the contributions that we miss have to do either with real emissions with widely separated jets, or virtual corrections where the gluon energy is not small with respect to the top mass. These corrections are in fact of two-loop level, and are not yet available.

The inclusion of bottom mass effects is more delicate. In this case, in fact, there is still factorization for light parton emissions at scale below the bottom mass. However, this scale is now much smaller than the Higgs mass, and such factorization may turn out not to be useful in most of the range of light parton emission, or of light parton virtualities in one-loop corrections. We thus consider two options in this case. In the first one we ignore this problem, and include the effect of the bottom quark in our rescaling factor. In the second option, we apply the top mass correction to all components of the cross section, but include the bottom mass effect only in the Born case.

The matrix elements for H +jet production at order α_s^3 and with full quark-mass dependence have been computed in ref. [28, 29], and are implemented in the POWHEG BOX in the generator `gg_H_quark-mass-effects` [35]. We have used the code of ref. [35] for our purposes.

We perform our reweighting at the level of the calculation of the matrix elements. The following reweighting factors are computed together with the Born term:

$$K_{tb} = \frac{B_{tb}(\Phi_B, m_t, m_b)}{B_{\text{inf}}}, \quad K_t = \frac{B_t(\Phi_B, m_t)}{B_{\text{inf}}}, \quad (2.1)$$

where

$$B_{\text{inf}} = B_{tb}(\Phi_B, m_t, m_b)|_{m_t=\infty, m_b=0}. \quad (2.2)$$

These reweighting factors are stored, and the Born matrix elements are multiplied by K_{tb} . The real and virtual corrections are multiplied by K_{tb} in our first option, and by K_t in our second option.²

We notice that with this procedure, the Born matrix element is computed with the exact quark-mass dependence. At variance with other methods, however, also the higher order terms are reweighted point by point in the phase space, either using the same reweighting factor, or a factor including only top mass effects. Our motivation to do so is that this is correct at least for the Born term and for the terms proportional to it.

2.2 Mass effects in the MiNLO procedure.

MiNLO [42] is in essence and extension of the well-known CKKW procedure [43] at the NLO level. One first associates a most likely branching history to the kinematic structure

¹The underlying Born kinematics of a given real emission kinematics configuration is obtained by an $n+1$ to n mapping procedure (specified in details in ref. [15, 16]) that is such that in the singular collinear limits corresponds to the Born kinematics of the factorized cross section.

²The Born matrix elements that are used to compute the real counterterms, the collinear remnants and the soft collinear terms are always rescaled in the same way as the real and virtual terms.

of the event. The hardness of the branchings are then used to set the factorization and renormalization scales. Furthermore, appropriate Sudakov form factors are supplied to the process, in full analogy with shower algorithms. Care has to be taken to subtract NLO terms arising from the expansion of the Sudakov form factor in order to maintain NLO accuracy of the cross section. The Sudakov form factors guarantee that the `MinLO` improved cross section can be integrated down to vanishing momenta of the associated jets. Furthermore, in ref. [21], it was shown that, in the case of the production of a boson in association with a jet, by a suitable refinement of the procedure, one could achieve NLO (i.e. α_s^3) accuracy for fully integrated quantities, i.e. even without requiring the presence of the jet.

The `MinLO` Sudakov form factor of ref. [21] is computed assuming that the main production vertex is pointlike, which is the case in the infinite top-mass approximation. This is a justified assumption if we only consider the top loop in the Higgs production vertex. Soft gluons are in fact characterized by energies below the Higgs mass. The flow of their momentum through the top loop is thus expected to have a very limited effect, in view of the large value of the top mass. On the other hand, also the bottom contributes to the Higgs coupling, with the interference of the bottom and top loop affecting the total cross section by about -7%. Furthermore, it was noticed that the `POWHEG` generator `gg_H_quark-mass-effects` yielded a transverse momentum distribution for the Higgs differing substantially with the analogous `MC@NLO` simulation, and with several analytic treatments of the Higgs transverse momentum spectrum. These differences are easily traced back to the fact that in `POWHEG` the Sudakov form factor is computed including the effects of the bottom finite mass. It is in fact given by the formula

$$\exp \left[- \int_{p'_T > p_T} \frac{R(\Phi_B, \Phi'_{\text{rad}})}{B(\Phi_B)} d\Phi'_{\text{rad}} \right], \quad (2.3)$$

where R is the real emission cross section and B is the Born term. On the other hand, in standard resummation formulae the real cross section is replaced by its Altarelli-Parisi approximation [44]. This assumes that the underlying Born cross section is not affected by virtualities of the incoming partons smaller than the Higgs mass.

This issue was dealt with in different ways in the literature. In ref. [39] it was assumed that the resummation scale in the case of bottom mediated Higgs production should have been set to the mass of the bottom rather than to the mass of the Higgs, in order to satisfy the basic resummation assumption that the soft gluons should be softer than the quark-mass. On the other hand, in ref. [40], it was shown by a detailed analytical study, that at order α_s^3 the double logarithmic structure of the gluon emission in Higgs production with quark-mass effects remains the same as in the infinite mass limit. There are however differences at the single logarithmic level. The all order logarithmic structure, accounting for the complex three-scales problem induced by the bottom contribution, is at present not known even at the double logarithmic level. It is thus clear that this fact will introduce an uncertainty in our current prediction that must be modeled in some way. In the present work, we do the following. We consider two possible approaches to the computation of the Higgs Sudakov form factor. In the first approach, that we will label as `MEMB` (standing for Matrix Elements m_b), we keep the same `MinLO` Sudakov that we use in the traditional

HJ-MiNLO generator, thus assuming that no large logarithms arise at order higher than α_s^3 due to the inclusion of the bottom mass effects. In the second approach, that we call RMB (standing for Resummed m_b), we assume that all what is present at order α_s^3 due to bottom mass effects exponentiates. In order to do this, for every Higgs production event, we multiply the MiNLO Sudakov form factor by

$$\Delta_{m_b}(p_{t,H}, y_H) = \exp \left[- \int_{p'_{t,H} > p_{t,H}} \left(\frac{R_{tb}}{B_{tb}} - \frac{R_t}{B_t} \right) d\Phi'_{\text{rad}} \right]. \quad (2.4)$$

Since

$$\int_{p'_{t,H} > p_{t,H}} \frac{R_t}{B_t} d\Phi'_{\text{rad}} \approx \int_{p'_{t,H} > p_{t,H}} \frac{R_{m_t=\infty}}{B_{m_t=\infty}} d\Phi'_{\text{rad}}, \quad (2.5)$$

we notice that if we use the Sudakov form factor of eq. (2.3), evaluated in the infinite quark-mass limit, instead of the MiNLO Sudakov, the Δ_{m_b} factor turns it into the Sudakov of eq. (2.3) including bottom mass effects. Thus, this second procedure should yield results that are closer to those of the `gg_H_quark-mass-effects` generator.

2.3 Quark-mass effects in HNNLO

Quark-mass effects have been implemented recently at NLO in the version 2 of the HNNLO [39] code. For the NNLO predictions used in this paper, we set `approxim=2` which corresponds to having exact top and bottom mass dependence at NLO and no approximate mass effects at NNLO.

3 Numerical study

We begin by considering the HJ-MiNLO generator, with the quark-mass effects included at different levels. We consider Higgs production at the 8 TeV LHC. We set $m_H = 125.5$ GeV, and use in the following MSTW2008NNLO parton distribution functions [45]. For the heavy quark-masses we use $m_t = 172.5$ GeV and $m_b = 3.38$ GeV. The choice of the bottom mass deserves some discussion.

3.1 The choice for the bottom mass.

In our computation, quark-mass renormalization plays no role. Thus, we have freedom in our choice of the quark-mass scheme that we should use, either an on-shell scheme, or the $\overline{\text{MS}}$ or DR scheme. The one-loop relation among the masses in the different schemes is as follows:

$$m_{\overline{\text{MS}}}(Q) = m_{\text{pole}} \times \left[1 - \frac{\alpha_s}{\pi} \left(\log \frac{Q^2}{m_{\text{pole}}^2} + 4/3 \right) + \mathcal{O}(\alpha_s^2) \right], \quad (3.1)$$

$$m_{\text{DR}}(Q) = m_{\text{pole}} \times \left[1 - \frac{\alpha_s}{\pi} \left(\log \frac{Q^2}{m_{\text{pole}}^2} + 5/3 \right) + \mathcal{O}(\alpha_s^2) \right]. \quad (3.2)$$

Choosing $\alpha_s = 0.115$ and $m_{\text{pole}} = 4.75$ GeV, for $Q = 125.5$ GeV we get 3.38 and 3.32 GeV for the $\overline{\text{MS}}$ and DR schemes respectively.

One could argue that, since the bottom appears in a loop involving momenta of the order of the Higgs mass, it should be more appropriate to use the bottom $\overline{\text{MS}}$ mass evaluated at the Higgs mass scale. The following observation also supports this view. We compute the Higgs total cross section $\sigma_t^{\text{LO|NLO}}$ (using the `gg_H_quark-mass-effects` generator) including only the top contribution at LO and NLO level. We then compute the same cross sections, $\sigma_{tb}^{\text{LO|NLO}}$, including also the bottom loop, in the $\overline{\text{MS}}$ and on-shell scheme. The results for the ratios are shown in table 1. We see that using the $\overline{\text{MS}}$ value at the LO level

	on-shell scheme	$\overline{\text{MS}}$ scheme
$\sigma_{tb}^{\text{LO}}/\sigma_t^{\text{LO}}$	0.89	0.93
$\sigma_{tb}^{\text{NLO}}/\sigma_t^{\text{NLO}}$	0.93	0.94

Table 1. Effect of the mass schemes on the inclusive Higgs cross section at LO and NLO level.

yields a mass effect that is closer to the one obtained at NLO. In the following, we will thus use the $\overline{\text{MS}}$ value. On the other hand, we have verified that changing the scheme for the top mass changes the cross section only at the per-mille level, both at LO and NLO.

3.2 Mass effects in matrix elements

For the following plots, we only consider results at the level of the Les Houches output, i.e. no shower effects are included.

First of all, we would like to assess the difference between the two variants for the implementation of mass corrections in the matrix elements, discussed in Sec.2.1, i.e. whether the bottom-mass correction should be only applied to the Born term, or to the full NLO cross-section. In figure 1 we compare the two procedures for both the Higgs rapidity dis-

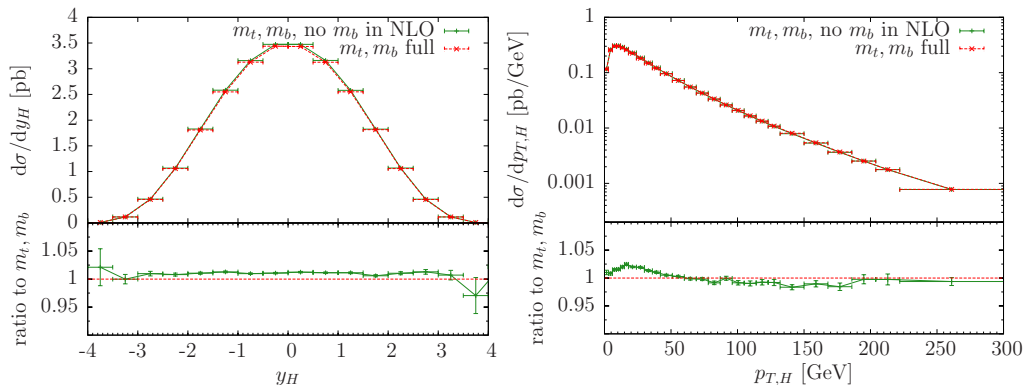


Figure 1. Rapidity and transverse momentum distributions for Higgs production at the 8 TeV LHC. The two lines represent the result from the HJ-MiNLO generator with bottom and top mass effects fully included in the matrix elements (red, dashed line), and the same generator without bottom mass effects in the matrix elements for the NLO corrections (green, solid).

tribution and the Higgs transverse momentum. As we can see, the differences are at most 2%. We will thus, as our default option, include also the bottom quark in the rescaling

factor for the NLO corrections. The other option is still provided in the public code. It can be used to assign a systematic error associated to using an approximated treatment of bottom-mass effects at NLO in HJ.

We now compare the plain HJ-MiNLO generator (without any quark-mass effects) to our new generator with mass effects included in the matrix elements only (and no mass effects included in the MiNLO Sudakov form factor), corresponding to our MEMB option. These are displayed in fig. 2 for the rapidity and transverse momentum distribution of the

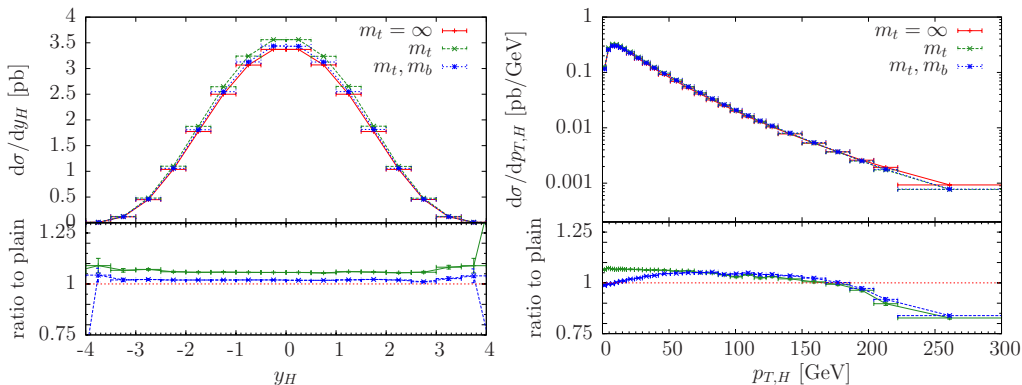


Figure 2. Rapidity and transverse momentum distributions for Higgs production at the 8 TeV LHC. The three lines represent the result from the plain HJ-MiNLO generator, and the result from the same generator improved with either the top mass effect alone, or with both top and bottom mass effects.

Higgs boson. From the rapidity distribution, we notice that the inclusion of the top mass alone amounts to a constant increase of about 5%. On the other hand, the inclusion of the bottom-mass effects decreases the cross section by about the same amount, thus yielding a net negligible effect on the total cross section. A very similar pattern is observed in the NLO total Higgs production inclusive cross section. For example, ref. [39] quotes a 6% increase due to the top mass, and a -1% effect when also bottom effects are included.

The similarity between the HJ-MiNLO and the fixed-order inclusive NLO results for the total cross section is not trivial. In fact, the HJ matrix elements are those for Higgs production in association with one parton at NLO, and with two partons at LO, while the fixed-order inclusive NLO case involves the matrix elements for the production of the Higgs without accompanying partons at NLO, plus the production of the Higgs with one extra parton at LO. In general, the MiNLO procedure guarantees that even when the extra partons in the HJ generator are integrated out, the same accuracy of the fixed order, inclusive NLO calculation is achieved. In the present case, since the mass corrections in HJ-MiNLO are included only in an approximate way, mass effects in the inclusive cross section do not have full NLO accuracy. As we can see, however, the same pattern of the NLO calculation is recovered. From the transverse momentum spectrum we notice that, as expected, the difference between including only the top, or both the top and the bottom quark is concentrated at low transverse momenta, below $p_{T,H} = 50$ GeV. At zero transverse momentum this difference is largest and amounts to about 12%.

3.3 Resummed mass effects

We still consider results at the Les Houches level, and compare the plain HJ-MiNLO generator (without any quark-mass effects) to our new generator with mass effects included in the matrix elements, and also including the correction to the MiNLO Sudakov given in eq. (2.5), corresponding to our RMB option.

Before doing so, we remind the reader that we expect these results to match to some extent those of the `gg_H_quark-mass-effects` generator. We thus begin by showing in fig. 3 results obtained with the `gg_H_quark-mass-effects`, when only the top loop is

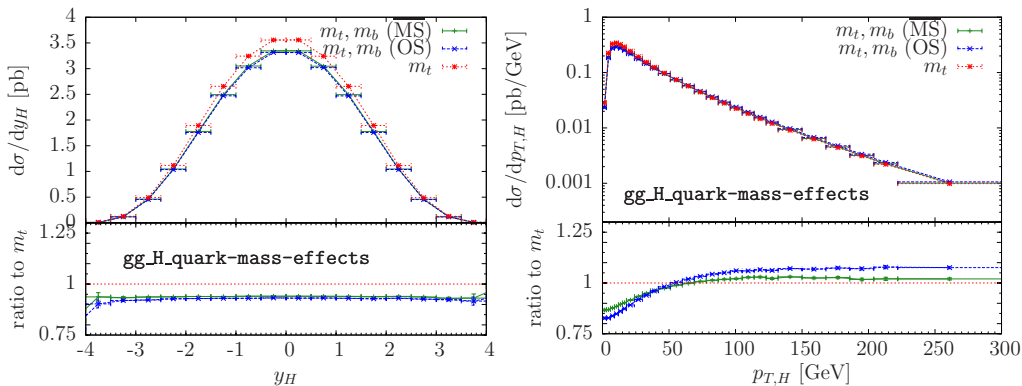


Figure 3. Rapidity and transverse momentum distributions for Higgs production at the 8 TeV LHC. The three lines represent the result from the `gg_H_quark-mass-effects` generator, when only the top loop is included, and when the bottom loop is added in the $\overline{\text{MS}}$ and in the on-shell scheme.

considered, in comparison to the case when also the bottom loop is included. In this last case, we display results in both schemes, the onshell and $\overline{\text{MS}}$ scheme. As explained before, in our opinion the latter choice is preferable in this case with respect to the on-shell scheme. We see that, in the $\overline{\text{MS}}$ scheme, in the rapidity distribution the difference is very small. This is due to the fact that scheme compensation takes place in inclusive quantities, i.e. the explicit modification of the virtual contribution due to the scheme change compensates the variation induced by the change in the mass parameter. This compensation does not take place in the transverse momentum distribution, that can be considered a leading order quantity, mostly affected directly by the change in the bottom mass. Furthermore, there is an explicit m_b dependence in the Sudakov exponent, where no scheme compensation occurs. In the onshell scheme we find more pronounced differences, both at low and high transverse momenta.

We now show in fig. 4 the HJ-MiNLO results in our RMB approach (red line) compared to including only top-mass effects (green line). As anticipated, the bottom-mass effect is now very similar to the one displayed in fig. 3.

3.4 NNLOPS results

We now turn to our full NNLOPS results. The NNLOPS events are showed with PYTHIA (v.6.4.25) with the 2011 Perugia tune (PYTUNE(350)). Results include full hadronization

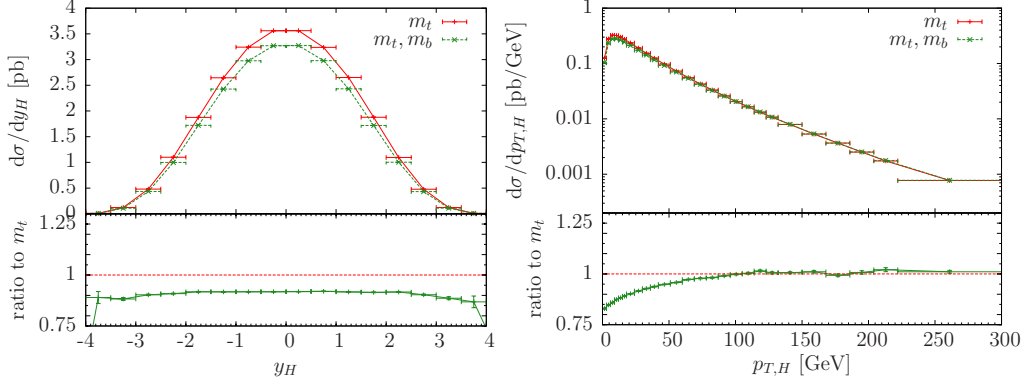


Figure 4. Rapidity and transverse momentum distributions for Higgs production at the 8 TeV LHC. The two lines represent the result from the HJ-MiNLO generator, when only the top loop is included, and when the bottom loop is added (in the $\overline{\text{MS}}$ scheme) in our RMB option.

and underlying event effects.

We start from the Higgs rapidity and transverse momentum distributions, that are displayed in fig. 5.

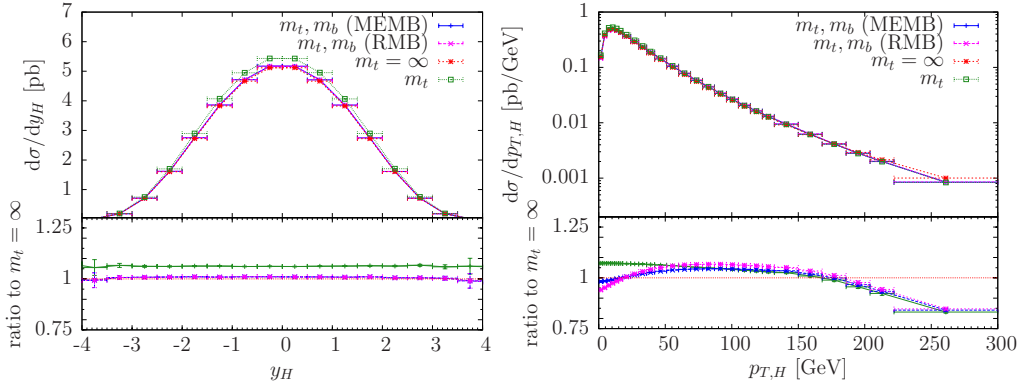


Figure 5. Rapidity and transverse momentum distributions for Higgs production at the 8 TeV LHC. The two lines represent the result from the NNLOPS generator, in the large m_t approximation (red), including only top-mass effects (green), and including top and bottom mass effects in the MEMB scheme (blue) or in the RMB scheme (magenta).

We see that, for the rapidity distribution the MEMB and RMB results are very close to each other, and in fact very close to the large m_t result. On the contrary, results including only top loops are about 6% larger. This is in fact the result that one obtains at pure NNLO level. In the transverse momentum distribution on the other hand, we observe a difference, of up to 5%, between the RMB and MEMB schemes.

In fig. 6 we show the four predictions for the leading jet integrated cross-section (left) and jet-veto efficiency (right). We notice that the difference between the MEMB and RMB schemes is very small (of the order of 1-2%) for values of the transverse momentum of the

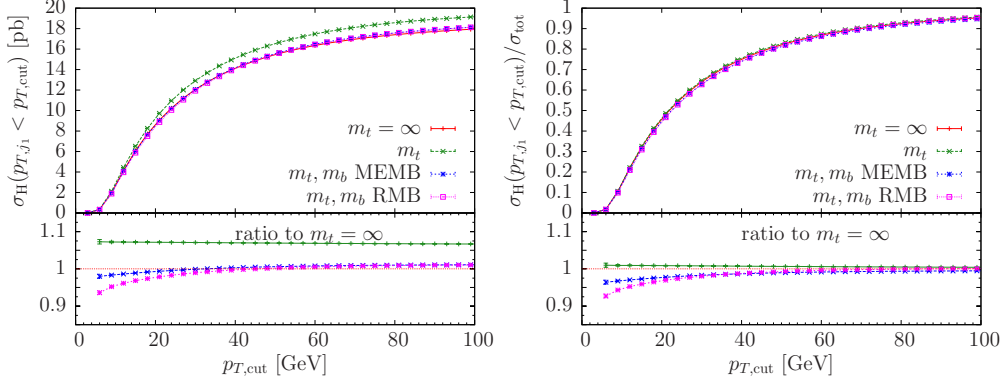


Figure 6. As in Fig. 5 but for the leading jet integrated cross-section (left) and jet-veto efficiency (right).

order of 25-30 GeV, the region of interest in Higgs studies involving a jet-veto in ATLAS and CMS. A similar conclusion was found in ref. [46] where a resummation for the jet-veto was presenting including various matching procedure to estimate the uncertainty due to the top-bottom interference contributions. On the other hand this difference rises at lower value of the jet-veto cut, and reaches about 5% at $p_{T,\text{cut}} = 5$ GeV.

Finally, in fig. 7 we show the effect of parton shower and hadronization for both the

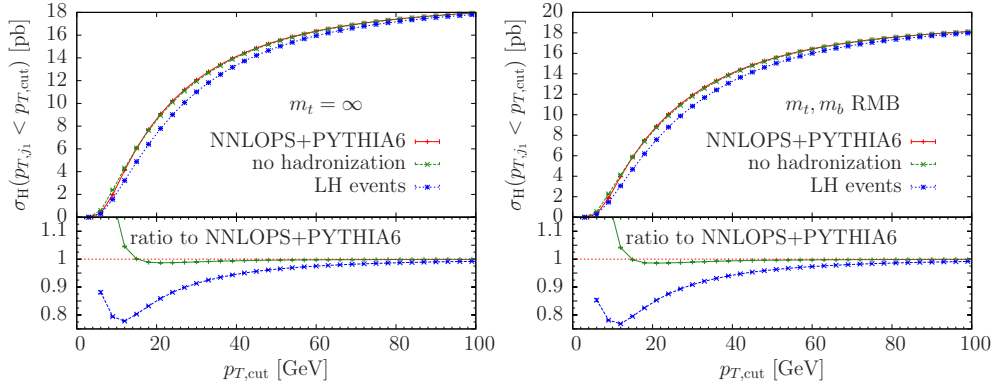


Figure 7. Comparison of the result after shower, hadronization and inclusion of the underlying event (red), after shower only (green), and at the Les Houches level (blue) for the leading jet integrated cross section. On the left, the $m_t = \infty$ result is shown, and on the right the RMB result is reported.

$m_t = \infty$ case and the m_t, m_b , RMB result. As we can see, the parton shower effect has a noticeable impact, while hadronization and the underlying event do not affect this observable sensibly. In this, we see no difference between the $m_t = \infty$ and the m_t, m_b , RMB case.

4 Conclusions

In this work, we have included finite quark-mass effects in our NNLOPS generator for Higgs production. As far as mass-corrections are concerned, the accuracy of our generator is that of currently available fixed-order calculations, i.e. NLO accuracy. In our procedure we have considered two possible sources of uncertainty. The first one, has to do with the fact that we rescale the full matrix elements with the mass effect that are computed at the level of Higgs production in association with one jet. This procedure may be considered safe as far as top mass-effects are concerned, where one may argue that dominant NLO corrections, involving momenta softer than the Higgs mass, will not affect the top-quark loop. This assumption is unjustified when the bottom loop is involved. We thus consider two alternatives: we either apply the mass-correction only to the Born contribution, or to the full NLO matrix element. We find that numerically, the two procedures lead to differences of the order of 2%. A second source of uncertainty has to do with the all-order inclusion of contributions enhanced by powers of $\log(m_b/m_H)$. Little is known about the all-order structure of these logarithms. We thus consider two options: either we do not include them at all, or we fully exponentiate them in the MiNLO Sudakov form factor. The first approach is similar in spirit to applying a resummation procedure by assuming that soft gluon momenta do not affect the quark loops. The second approach is analogous to what is implemented in the `gg_H_quark-mass-effects` generator, where the POWHEG procedure leads to full exponentiation of the real emission cross-section including mass effects. In this case we find differences in the low transverse momentum region of the order of 5% starting from the low momentum region and changing direction at high transverse momenta. On the other hand, when considering jet-veto distributions for typical values of the transverse momentum cuts used by ATLAS and CMS ($p_{T,\text{cut}} = 25\text{-}30$ GeV), we find only 1-2% differences.

Unlike in ref. [17] we have not reported here a study of scale variation, since in view of the smallness of the quark-mass effects, we do not expect to get results sensibly different from those of reference [17].

The code for this generator has been made available in an update of the HJ package in the POWHEG-BOX-V2.

Acknowledgments

The research of GZ is supported by the Consolidator ERC Grant 614577. We would like to thank the Galileo Galilei Institute (PN and GZ) and CERN (PN) for hospitality while part of this work was carried out. KH is grateful to the Institute for Particle Physics Phenomenology in Durham, for support in the form of an IPPP Associateship.

A Technical details about b -mass effects in the MiNLO Sudakov

The inclusion of bottom-mass effects in the MiNLO Sudakov, following eq. (2.5), requires for each point an additional integration over a ratio a matrix elements, for fixed y_H , over

the phase space region where the Higgs transverse momentum is larger than the Higgs transverse momentum of the event, p_T . Since such integration is performed on the fly for each point, it is crucial that the phase space is sampled efficiently. Furthermore, we will use an approximate expression of the matrix elements appearing in eq.(2.5). In Appendix A.1 we give all details about the phase space evaluation, while in Appendix A.2 we illustrate the approximations done on the matrix elements in eq. (2.5).

A.1 Phase space

Here we study the phase space integration of the matrix element for the production of a Higgs boson plus one light parton, under the constraint that the Higgs boson has fixed rapidity y_H , and that its transverse momentum is larger than a given lower limit p_T .

We denote by m_H the Higgs mass, $k_H = (E, \mathbf{k})$ its four momentum, by $l_g = (l, \mathbf{l})$ the light-parton momentum and define $q = k_H + l_g$. The three-vectors \mathbf{l} and \mathbf{k} are defined in the partonic center of mass (CM) frame. We have also defined $k = |\mathbf{k}|$ and $l = |\mathbf{l}|$. The two body phase space in the rest frame of the Higgs-light-parton system is then given by:

$$\begin{aligned} d\Phi_2 &= \frac{d^3\mathbf{l}}{2l(2\pi)^3} 2\pi\delta((q - l_g)^2 - m_H^2) \\ &= \frac{d^3\mathbf{l}}{2l(2\pi)^2} \delta(q^2 - m_H^2 - 2q^0l) = \frac{d^2l_T dl_l}{2l(2\pi)^2} \delta\left(q^2 - m_H^2 - 2q^0\sqrt{l_T^2 + l_l^2}\right) \\ &= \sum_{\pm} \frac{1}{16\pi} \frac{\theta(l^2 - l_T^2)}{\sqrt{s}\sqrt{l^2 - l_T^2}} dl_T^2 = \sum_{\pm} \frac{1}{16\pi} \frac{\theta(k^2 - k_T^2)}{\sqrt{s}\sqrt{k^2 - k_T^2}} dk_T^2, \end{aligned} \quad (\text{A.1})$$

where $s = q^2$ and where we have used the property $\mathbf{k} = -\mathbf{l}$. The \pm sum refers to the two possible signs of the l_l integral (the suffix l stands here for longitudinal).

The full phase space integral, to be multiplied by parton distribution functions and partonic cross section, including the constraint that the Higgs transverse momentum is larger than p_T , is then

$$\int dk_T^2 \sum_{\pm} \frac{1}{16\pi} \frac{1}{\sqrt{s}\sqrt{k^2 - k_T^2}} \int dy_{\text{cm}} d\tau \delta(\pm y_{\text{cm}}^H - (y^H - y_{\text{cm}})) \theta(k^2 - k_T^2) \theta(k_T^2 - p_T^2), \quad (\text{A.2})$$

where y^H is the Higgs rapidity in the laboratory frame and y_{cm}^H the Higgs rapidity in the CM frame. The above expression is equivalent to

$$\int dk_T^2 \frac{1}{16\pi} \frac{1}{\sqrt{s}\sqrt{k^2 - k_T^2}} \int dy_{\text{cm}} d\tau \delta(y_{\text{cm}}^H - |y^H - y_{\text{cm}}|) \theta(k^2 - k_T^2) \theta(k_T^2 - p_T^2). \quad (\text{A.3})$$

The Higgs rapidity in the CM frame can be written as

$$y_{\text{cm}}^H = \frac{1}{2} \log \frac{E + \sqrt{k^2 - k_T^2}}{E - \sqrt{k^2 - k_T^2}}, \quad (\text{A.4})$$

where E, k are the energy and momentum of the Higgs in the partonic CM frame:

$$E = \frac{s + m_H^2}{2\sqrt{s}} = m_H \frac{1+z}{2\sqrt{z}}, \quad k = \frac{s - m_H^2}{2\sqrt{s}} = m_H \frac{1-z}{2\sqrt{z}}, \quad (\text{A.5})$$

and $s = m_H^2/z$. Furthermore we define

$$\tau = \frac{s}{S} = \frac{m_H^2}{Sz}. \quad (\text{A.6})$$

In order to solve for k_T^2 in the delta function we get

$$\sqrt{k^2 - k_T^2} = E \tanh |y_H - y_{\text{cm}}|, \quad (\text{A.7})$$

and

$$k_T^2 = k^2 - E^2 \tanh^2(y_H - y_{\text{cm}}). \quad (\text{A.8})$$

Since we must have $p_T < k_T < k$, from the theta functions we get the constraints

$$p_T^2 < k^2 - E^2 \tanh^2(y_H - y_{\text{cm}}) < k^2, \quad (\text{A.9})$$

that is to say

$$k^2 - p_T^2 > E^2 \tanh^2(y_H - y_{\text{cm}}), \quad (\text{A.10})$$

or

$$\Delta y \equiv \text{atanh} \sqrt{\frac{k^2 - p_T^2}{E^2}} = \frac{1}{2} \log \left(\frac{E + \sqrt{k^2 - p_T^2}}{E - \sqrt{k^2 - p_T^2}} \right) > |y_H - y_{\text{cm}}|. \quad (\text{A.11})$$

The jacobian for the delta function integration is

$$\left| \frac{\partial y_{\text{cm}}^H}{\partial k_T^2} \right|^{-1} = \frac{2}{E} (E^2 - k^2 + k_T^2) \sqrt{k^2 - k_T^2} = \frac{2(m_H^2 + k_T^2) \sqrt{k^2 - k_T^2}}{E}. \quad (\text{A.12})$$

Our phase space integral becomes

$$\int d\tau \int_{\frac{1}{2} \log \tau}^{-\frac{1}{2} \log \tau} dy_{\text{cm}} \frac{1}{8\pi} \frac{E^2 - k^2 + k_T^2}{E\sqrt{s}} \theta(\Delta y - |y_H - y_{\text{cm}}|) \theta(k^2 - p_T^2), \quad (\text{A.13})$$

which is equivalent to

$$\int_{\tau_0}^1 d\tau \int_{\frac{1}{2} \log \tau}^{\frac{1}{2} \log 1/\tau} dy_{\text{cm}} \frac{z}{4\pi} \frac{m_H^2 + k_T^2}{m_H^2(1+z)} \theta(k^2 - E^2 \tanh^2(y_H - y_{\text{cm}}) - p_T^2), \quad (\text{A.14})$$

with $\tau_0 = (p_T + M_T)^2/S$, with $M_T = \sqrt{p_T^2 + m_H^2}$. This limit arises from the requirement:

$$k = \frac{s - m_H^2}{2\sqrt{s}} > p_T, \quad (\text{A.15})$$

that implies

$$s - 2\sqrt{s}p_T - m_H^2 > 0 \Rightarrow (\sqrt{s} - (p_T + M_T)) (\sqrt{s} - (p_T - M_T)) > 0, \quad (\text{A.16})$$

which in turn implies

$$s > (p_T + M_T)^2. \quad (\text{A.17})$$

The theta function

$$\theta(k^2 - E^2 \tanh^2(y_H - y_{\text{cm}}) - p_T^2) \quad (\text{A.18})$$

also implies some restrictions on y_{cm} , that we now work out. It can be written as

$$\text{atanh} \sqrt{\frac{k^2 - p_T^2}{E^2}} > |y_H - y_{\text{cm}}|, \quad (\text{A.19})$$

or

$$y_H + \Delta > y_{\text{cm}} > y_H - \Delta, \quad (\text{A.20})$$

with

$$\Delta = \text{atanh} \sqrt{\frac{k^2 - p_T^2}{E^2}}. \quad (\text{A.21})$$

Combined with the integration limits for y_{cm} , this yields

$$\max\left(-\frac{1}{2} \log \frac{1}{\tau}, y_H - \Delta\right) < y_{\text{cm}} < \min\left(\frac{1}{2} \log \frac{1}{\tau}, y_H + \Delta\right). \quad (\text{A.22})$$

The range is not empty if

$$\begin{aligned} -\frac{1}{2} \log \frac{1}{\tau} &< y_H + \Delta, \\ y_H - \Delta &< \frac{1}{2} \log \frac{1}{\tau}, \end{aligned}$$

that can be combined into

$$\Delta > -\frac{1}{2} \log \frac{1}{\tau} + |y_H|. \quad (\text{A.23})$$

Taking the hyperbolic tangent of both sides we get

$$\sqrt{\frac{k^2 - p_T^2}{E^2}} > \frac{\tau e^{2|y_H|} - 1}{\tau e^{2|y_H|} + 1} = \frac{\tau - e^{-2|y_H|}}{\tau + e^{-2|y_H|}}. \quad (\text{A.24})$$

Let us define $\eta = e^{-2|y_H|}$; we have the inequality

$$\sqrt{\frac{k^2 - p_T^2}{E^2}} > \frac{\tau - \eta}{\tau + \eta}, \quad (\text{A.25})$$

or

$$\sqrt{\frac{(\tau S - m_H^2)^2 - 4S p_T^2 \tau}{(\tau S + m_H^2)^2}} > \frac{\tau - \eta}{\tau + \eta}, \quad (\text{A.26})$$

that is easily solved to yield either $\tau < \eta$, or

$$\tau > \tau_1 = \frac{(\eta S - m_H^2) \sqrt{\eta S M_T^2 + \eta S p_T^2}}{S(\eta S - M_T^2)}, \quad (\text{A.27})$$

or

$$\tau < \tau_2 = \frac{-(\eta S - m_H^2)\sqrt{\eta S M_T^2 + \eta S p_T^2}}{S(\eta S - M_T^2)}. \quad (\text{A.28})$$

Setting $\eta = x^2$, and using $S = E^2$ and $m_H^2 = M_T^2 - p_T^2$, we get (using an algebraic manipulation code)

$$\tau_1 = \frac{x(EM_T x + p_T^2 + M_T^2)}{E(Ex + M_T)}, \quad (\text{A.29})$$

$$\tau_2 = -\frac{x(EM_T x - p_T^2 + M_T^2)}{E(Ex + M_T)} < 0, \quad (\text{A.30})$$

so that only τ_1 is retained, and we need to satisfy the conditions: either $\tau > \tau_0$ and $\tau < \eta$, or $\tau > \tau_0$ and $\tau > \tau_1$. We also find:

$$\tau_1 - \eta = -x \frac{(Ex - p_T - M_T)(Ex + p_T - M_T)}{E(Ex - M_T)} = -x(x - \sqrt{\tau_0}) \frac{Ex + p_T - M_T}{Ex - M_T}, \quad (\text{A.31})$$

and

$$\tau_1 - \tau_0 = \frac{M_T(x - \sqrt{\tau_0})^2}{Ex - M_T} \quad (\text{A.32})$$

We notice that we must have $Ex - M_T > 0$ in all cases, otherwise the Higgs with transverse mass M_T and rapidity y_H would be inconsistent with the total incoming energy. Hence $\tau_1 > \tau_0$, and we get only two cases:

1. $\tau_0 < \eta$: in this case the right hand side of eq. (A.31) is negative. In fact, $E\sqrt{\tau_0} - M_T$ is obviously positive, and it remain positive if we replace $\sqrt{\tau_0}$ with x , since $x > \sqrt{\tau_0}$. So the last factor on the right hand side of eq. (A.31) is positive, and the right hand side is negative. Therefore $\tau_1 < \eta$, and the range of integration in τ is $\tau_0 < \tau < 1$, because $\tau > \eta$ also implies $\tau > \tau_1$.
2. $\tau_0 > \eta$: in this case eq. (A.32) guarantees that $\tau_1 > \tau_0$, and we have $\tau_1 > \tau_0 > \eta$. The range of integration is $\tau_1 < \tau < 1$. The condition $\tau_1 < 1$ is the remaining requirement of consistency for the assigned y_H and p_T values.

A.2 Approximate matrix elements in the MiNLO Sudakov

Here we record the approximate matrix elements used for computing our finite quark-mass corrections to the MiNLO Sudakov form factor. For what concerns quark-mass effects in the partonic Higgs boson-plus-one parton sub-processes, all other components entering the construction of our NNLOPS event generator utilize the exact, leading order, $2 \rightarrow 2$ matrix elements. Since the $qq \rightarrow Hg$ matrix element contains no enhanced terms proportional to $1/p_T^2$, it cannot give rise to corrections to the Sudakov form factor, hence it does not feature here.

The pure b -quark loop mediated contributions to the p_T spectrum are greatly suppressed by a factor m_b^2/m_H^2 relative to those owing to the interference of the t - and b -loop mediated amplitudes, hence, our first approximation has been to neglect the former. Our second simplification is to use the relatively simpler small quark-mass limit of the scalar

loop integrals given in ref. [29] for the b -loop amplitudes, while using the large- m_t limit for the top-loop amplitudes. The small quark-mass limit of ref. [29] is defined by taking m_b as being small compared to all other kinematic invariants in the process.

We have validated the following approximate matrix elements numerically in various ways. To begin with we have compared them point-wise in phase space to the exact matrix elements. In the latter case the evaluation of the *integrand* in the correction to the Sudakov exponent, modulo convolution with the PDFs, with the approximate matrix elements agrees with its exact analogue to well within 20% for $20 \lesssim p_T \lesssim 150$ GeV. For $gg \rightarrow Hg$ and $gq \rightarrow Hq$ channels the approximate matrix elements are particularly effective, and agreement in that case is better than 10% for $10 \ll p_T \ll 300$ GeV. Since all of our matrix element approximations involve the small- m_b limit, they can all be expected to breakdown for $p_T \rightarrow m_b$, however, to perform the proposed correction to the Sudakov form factor, which involves the cumulant in p_T starting at its maximum value, this breakdown is unimportant. We have also tested the approximate matrix elements against their exact counterparts in the evaluation of the full correction to the Sudakov form factor itself, $\Delta_{m_b}(p_T, y_H)$. Due to the fact this quantity involves an integral over p_T up to its maximum attainable value, and the convolution of the matrix elements with the PDFs — marginalising the contribution of the high $p_T \gtrsim m_t$ region, in which the $gg \rightarrow Hg$ approximation loses quality — we find that results for $\Delta_{m_b}(p_T, y_H)$ obtained using the approximate matrix elements are almost indistinguishable from those found using the exact matrix elements.

A.2.1 Preliminaries

The exact spin-colour averaged Born amplitude squared, including finite top- and bottom-quark-mass effects, $\mathcal{M}_{gg \rightarrow H}^{[m_t, m_b]}$, and its large- m_t limit, $\mathcal{M}_{gg \rightarrow H}^{[\infty, 0]}$, are given by,

$$\mathcal{M}_{gg \rightarrow H}^{[\infty, 0]} = \frac{G_F m_H^4 \alpha_S^2}{288 \sqrt{2} \pi^2} \quad \text{and} \quad \mathcal{M}_{gg \rightarrow H}^{[m_t, m_b]} = \mathcal{F} \mathcal{M}_{gg \rightarrow H}^{[\infty, 0]}, \quad (\text{A.33})$$

where,

$$\mathcal{F} = \left| \sum_q \frac{3}{2\tau_q^2} (\tau_q + (\tau_q - 1) f(\tau_q)) \right|^2, \quad f(\tau_q) = \begin{cases} \arcsin^2 \sqrt{\tau_q} & \tau_q \leq 1, \\ -\frac{1}{4} \left[\log \frac{1 + \sqrt{1 - 1/\tau_q}}{1 - \sqrt{1 - 1/\tau_q}} - i\pi \right]^2 & \tau_q > 1, \end{cases} \quad (\text{A.34})$$

with $\tau_q = \frac{1}{4} m_H^2 / m_q^2$ and m_q being the mass of the quark ($q = t, b$). In the large- m_t -small- m_b limit,

$$\lim_{\substack{m_t \rightarrow \infty \\ m_b \rightarrow 0}} \mathcal{F} \rightarrow 1 + \frac{3}{4} \tau_b^{-1} \mathcal{F}_{tb} + \mathcal{O}(\tau_b^{-2}), \quad \mathcal{F}_{tb} = 4 + \pi^2 - \log^2(4\tau_b). \quad (\text{A.35})$$

In eq. (A.35) the leading term (1) arises from pure top-loop mediated $gg \rightarrow H$ amplitudes, the second term proportional to τ_b^{-1} owes to the interference of top- with bottom-quark loop $gg \rightarrow H$ amplitudes. To evaluate finite mass corrections to the Sudakov form factor we neglect terms $\mathcal{O}(\tau_b^{-2})$, arising from pure b -loop mediated contributions.

For the pole b -quark-mass, $m_b = 4.75$ GeV, and $m_H = 125$ GeV we find $\frac{3}{4} \mathcal{F}_{tb} \tau_b^{-1} = -0.125$, while taking instead the $\overline{\text{MS}}$ b -quark-mass, $m_b = 3.38$ GeV, leads to $\frac{3}{4} \mathcal{F}_{tb} \tau_b^{-1} = -0.084$.

A.2.2 $qg \rightarrow Hq$ and $qg \rightarrow Hq$ approximate matrix elements

Neglecting bottom quark contributions, in the large- m_t limit the $qg \rightarrow Hq$ matrix element is given by,

$$\mathcal{M}_{qg \rightarrow Hq}^{[\infty,0]} = \mathcal{M}_{qg \rightarrow H}^{[\infty,0]} \left(\frac{8\pi\alpha_s C_F}{m_H^4} \right) \frac{t^2 + s^2}{|u|}. \quad (\text{A.36})$$

Our approximate $2 \rightarrow 2$ matrix element for $qg \rightarrow Hq$ is obtained by taking the large- m_t -small- m_b limit of the full $qg \rightarrow Hq$ matrix element including top- and bottom-quark mediated contributions. We express it in terms of a piece, $\mathcal{M}_{qg \rightarrow Hq}^{\mathcal{F}}$, which respects conventional soft and collinear factorisation, and a further remainder term, $\mathcal{M}_{qg \rightarrow Hq}^{\mathcal{R}}$, which does not:

$$\lim_{\substack{m_t \rightarrow \infty \\ m_b \rightarrow 0}} \mathcal{M}_{qg \rightarrow Hq}^{[m_t, m_b]} \rightarrow \mathcal{M}_{qg \rightarrow Hq}^{\mathcal{A}} = \mathcal{M}_{qg \rightarrow Hq}^{\mathcal{F}} + \mathcal{M}_{qg \rightarrow Hq}^{\mathcal{R}} \quad (\text{A.37})$$

where,

$$\mathcal{M}_{qg \rightarrow Hq}^{\mathcal{F}} = \mathcal{M}_{qg \rightarrow Hq}^{[\infty,0]} \left(1 + \frac{3}{4} \tau_b^{-1} \mathcal{F}_{tb} \right), \quad (\text{A.38})$$

$$\mathcal{M}_{qg \rightarrow Hq}^{\mathcal{R}} = \mathcal{M}_{qg \rightarrow Hq}^{[\infty,0]} \frac{m_H^2}{|u| + m_H^2} \frac{3}{4} \tau_b^{-1} \left[-\frac{|u|}{m_H^2} \mathcal{F}_{tb} + \log^2 \frac{m_b^2}{|u| + \varepsilon} - \frac{4|u|}{|u| + m_H^2} \log \frac{|u|}{m_H^2} \right] \quad (\text{A.39})$$

with $\varepsilon = m_b^2$ inserted by-hand, to regulate the potential divergence in the region where our small- m_b approximation breaks down.

We note how, in the approximate matrix element here, the interference of the top- and bottom-quark loop contribution vanishes at high $|u|$. Since the top-loop amplitude contribution to $qg \rightarrow Hq$ is manifestly real in the large- m_t limit, the vanishing interference at high $|u|$ implies the bottom-quark loop amplitude is pure-imaginary, i.e. the latter is dominated by real rescattering at high energy.

In the limit of large u (backward-scattering of the incoming quark) the large- m_t limit, severely fails to describe the Higgs boson's transverse momentum for intermediate p_T . On the other hand, the quark-mass dependence of the purely top-quark mediated contribution can be captured by a relatively simple formula:

$$\begin{aligned} \mathcal{M}_{qg \rightarrow Hq}^{[m_t, 0]} &= \mathcal{M}_{qg \rightarrow Hq}^{[\infty, 0]} \times \frac{36m_t^4}{(m_H^2 + |u|)^4} \left[-|u| - m_H^2 \right. \\ &\quad - 2|u| \left(\sqrt{\frac{4m_t^2}{m_H^2} - 1} \sin^{-1} \left(\frac{1}{2} \sqrt{\frac{m_H^2}{m_t^2}} \right) - \sqrt{1 + \frac{4m_t^2}{|u|}} \sinh^{-1} \left(\frac{1}{2} \sqrt{\frac{|u|}{m_t^2}} \right) \right) \\ &\quad \left. + (4m_t^2 - s - t) \left(\sin^{-1} \left(\frac{1}{2} \sqrt{\frac{m_H^2}{m_t^2}} \right)^2 + \sinh^{-1} \left(\frac{1}{2} \sqrt{\frac{|u|}{m_t^2}} \right)^2 \right) \right]^2. \quad (\text{A.40}) \end{aligned}$$

The approximate matrix element implemented is given by the rescaling

$$\mathcal{M}_{qg \rightarrow Hq}^{\mathcal{A}} \rightarrow \frac{\mathcal{M}_{qg \rightarrow Hq}^{[m_t, 0]}}{\mathcal{M}_{qg \rightarrow Hq}^{[\infty, 0]}} \times \mathcal{M}_{qg \rightarrow Hq}^{\mathcal{A}}. \quad (\text{A.41})$$

The analogous $gq \rightarrow Hq$ matrix element is readily obtained by substituting $u \leftrightarrow t$ in the $qg \rightarrow Hq$ formulae above.

A.2.3 $gg \rightarrow Hg$ approximate matrix element

Neglecting bottom quark contributions, in the large- m_t limit the $gg \rightarrow Hg$ matrix element is given by,

$$\mathcal{M}_{gg \rightarrow Hg}^{[\infty,0]} = \mathcal{M}_{gg \rightarrow H}^{[\infty,0]} \left(\frac{8\pi\alpha_s 2N_C}{m_H^4} \right) \frac{m_H^8 + s^4 + t^4 + u^4}{2stu}. \quad (\text{A.42})$$

Omitting terms $\mathcal{O}(\tau_b^{-2})$, in the large- m_t -small- m_b approximation, we go on and take the limit $m_b \ll p_T \ll m_H$, keeping only the resulting leading $\log^2 m_b^2$ term in the top-bottom interference piece we obtain

$$\lim_{\substack{m_t \rightarrow \infty \\ m_b \rightarrow 0 \\ m_b \ll p_T \ll m_H}} \mathcal{M}_{gg \rightarrow Hg}^{[m_t, m_b]} \rightarrow \mathcal{M}_{gg \rightarrow Hg}^{\mathcal{F}} + \mathcal{M}_{gg \rightarrow Hg}^{\mathcal{R}}, \quad (\text{A.43})$$

where,

$$\mathcal{M}_{gg \rightarrow Hg}^{\mathcal{F}} = \mathcal{M}_{gg \rightarrow Hg}^{[\infty,0]} \left(1 + \frac{3}{4} \mathcal{F}_{tb} \tau_b^{-1} \right), \quad (\text{A.44})$$

$$\mathcal{M}_{gg \rightarrow Hg}^{\mathcal{R}} = \mathcal{M}_{gg \rightarrow H}^{[\infty,0]} \left(\frac{8\pi\alpha_s 2N_C}{p_T^2} \right) \frac{1}{z^2} \frac{3}{4} \tau_b^{-1} (1-z) \left(1 - z + \frac{5}{4} z^2 \right) \log^2 \left(\frac{m_b^2}{p_T^2} \right). \quad (\text{A.45})$$

For $z \rightarrow 1$ this approximation recovers the results of conventional soft eikonal factorisation at the level of the pure t -loop mediated contribution, as well as for those terms above originating from t - b interference. The vanishing of the factorization-breaking remainder pieces as $z \rightarrow 1$, is consistent with Sec. 3.1 of ref. [40] concerning soft factorisation. The formulae here extend those of ref. [40], giving a unified description of soft and collinear regions.

Starting from the large- m_t -small- m_b approximation and taking instead just the $z \rightarrow 0$ high energy limit, neglecting terms $\mathcal{O}(1/z)$ gives formulae with a structure strongly resembling of the large- m_t -small- m_b approximation applied to the $qg \rightarrow Hq$ and $gq \rightarrow Hq$ channels eqs. (A.38, A.39):

$$\lim_{\substack{m_t \rightarrow \infty \\ m_b \rightarrow 0 \\ z \rightarrow 0}} \mathcal{M}_{gg \rightarrow Hg}^{[m_t, m_b]} \rightarrow \mathcal{M}_{gg \rightarrow Hg}^{\mathcal{F}'} + \mathcal{M}_{gg \rightarrow Hg}^{\mathcal{R}'}, \quad (\text{A.46})$$

where,

$$\mathcal{M}_{gg \rightarrow Hg}^{\mathcal{F}'} = \mathcal{M}_{gg \rightarrow Hg}^{[\infty,0]} \left(1 + \frac{3}{4} \mathcal{F}_{tb} \tau_b^{-1} \right), \quad (\text{A.47})$$

$$\mathcal{M}_{gg \rightarrow Hg}^{\mathcal{R}'} = \mathcal{M}_{gg \rightarrow Hg}^{[\infty,0]} \frac{m_H^2}{p_T^2 + m_H^2} \frac{3}{4} \tau_b^{-1} \left[-\frac{p_T^2}{m_H^2} \mathcal{F}_{tb} + \log^2 \left(\frac{m_b^2}{p_T^2} \right) - \frac{4p_T^2}{p_T^2 + m_H^2} \log \left(\frac{p_T^2}{m_H^2} \right) \right] \quad (\text{A.48})$$

Our final approximate matrix element expression for $gg \rightarrow Hg$ is made by combining those for the $m_b \ll p_T \ll m_H$ and $z \rightarrow 0$ domains into a single formula respecting both limits and interpolating between them:

$$\mathcal{M}_{gg \rightarrow Hg}^{[m_t, m_b]} \rightarrow \mathcal{M}_{gg \rightarrow Hg}^{\mathcal{A}} = \frac{\mathcal{M}_{gg \rightarrow H}^{[m_t, 0]}}{\mathcal{M}_{gg \rightarrow H}^{[\infty, 0]}} [\mathcal{M}_{gg \rightarrow Hg}^{\mathcal{F}} + \mathcal{M}_{gg \rightarrow Hg}^{\mathcal{R}}], \quad (\text{A.49})$$

with

$$\mathcal{M}_{gg \rightarrow Hg}^{\mathcal{F}} = \mathcal{M}_{gg \rightarrow Hg}^{[\infty, 0]} \left(1 + \frac{3}{4} \mathcal{F}_{tb} \tau_b^{-1} \right), \quad (\text{A.50})$$

$$\begin{aligned} \mathcal{M}_{gg \rightarrow Hg}^{\mathcal{R}} &= \mathcal{M}_{gg \rightarrow Hg}^{[\infty, 0]} \frac{m_H^2}{p_T^2 + m_H^2} \frac{3}{4} \tau_b^{-1} \\ &\times \left[-\frac{p_T^2}{m_H^2} \mathcal{F}_{tb} + \frac{\frac{1}{z} (1 - z + \frac{5}{4} z^2)}{z(1-z) + \frac{1-z}{z} + \frac{z}{1-z}} \log^2 \left(\frac{m_b^2}{p_T^2 + \varepsilon} \right) - \frac{4p_T^2}{p_T^2 + m_H^2} \log \left(\frac{p_T^2}{m_H^2} \right) \right]. \end{aligned} \quad (\text{A.51})$$

As in eq. (A.39), $\varepsilon = m_b^2$ has been inserted by-hand in eq. (A.51) to regulate the spurious divergence in the region where our small- m_b approximation breaks down. The ratio $\mathcal{M}_{gg \rightarrow H}^{[m_t, 0]} / \mathcal{M}_{gg \rightarrow H}^{[\infty, 0]}$ appears in eq. (A.49) as an economical bid to capture some of the finite top-quark mass dependence.

References

- [1] **ATLAS Collaboration** Collaboration, G. Aad et al., *Observation of a new particle in the search for the Standard Model Higgs boson with the ATLAS detector at the LHC*, *Phys.Lett.* **B716** (2012) 1–29, [[arXiv:1207.7214](#)].
- [2] **CMS Collaboration** Collaboration, S. Chatrchyan et al., *Observation of a new boson at a mass of 125 GeV with the CMS experiment at the LHC*, *Phys.Lett.* **B716** (2012) 30–61, [[arXiv:1207.7235](#)].
- [3] **CMS Collaboration**, *Update on the search for the standard model Higgs boson in pp collisions at the LHC decaying to W + W in the fully leptonic final state*, *CMS-PAS-HIG-13-003* (2013).
- [4] **CMS Collaboration**, S. Chatrchyan et al., *Search for a Higgs boson decaying into a Z and a photon in pp collisions at $\sqrt{s} = 7$ and 8 TeV*, *Phys.Lett.* **B726** (2013) 587–609, [[arXiv:1307.5515](#)].
- [5] **CMS Collaboration**, S. Chatrchyan et al., *Evidence for the 125 GeV Higgs boson decaying to a pair of τ leptons*, *JHEP* **1405** (2014) 104, [[arXiv:1401.5041](#)].
- [6] **CMS Collaboration**, *Search for SM Higgs in WH to WWW to 3l 3nu*, *CMS-PAS-HIG-13-009* (2013).
- [7] **CMS Collaboration**, V. Khachatryan et al., *Precise determination of the mass of the Higgs boson and tests of compatibility of its couplings with the standard model predictions using proton collisions at 7 and 8 TeV*, [[arXiv:1412.8662](#)].
- [8] **ATLAS Collaboration**, *Measurements of the properties of the Higgs-like boson in the two photon decay channel with the ATLAS detector using 25 fb⁻¹ of proton-proton collision data*, *ATLAS-CONF-2013-012*, *ATLAS-COM-CONF-2013-015* (2013).

- [9] **ATLAS** Collaboration, *Search for a Standard Model Higgs boson in $H \rightarrow \mu\mu$ decays with the ATLAS detector.*, *ATLAS-CONF-2013-010*, *ATLAS-COM-CONF-2013-003* (2013).
- [10] **ATLAS** Collaboration, *Search for the Standard Model Higgs boson in the $H \rightarrow Z\gamma$ decay mode with pp collisions at $\sqrt{s} = 7$ and 8 TeV*, *ATLAS-CONF-2013-009*, *ATLAS-COM-CONF-2013-014* (2013).
- [11] *Study of the spin of the new boson with up to 25 fb^{-1} of atlas data*, Tech. Rep. ATLAS-CONF-2013-040, CERN, Geneva, Apr, 2013.
- [12] **ATLAS Collaboration** Collaboration, G. Aad et al., *Measurements of fiducial and differential cross sections for Higgs boson production in the diphoton decay channel at $\sqrt{s} = 8$ TeV with ATLAS*, *JHEP* **1409** (2014) 112, [[arXiv:1407.4222](#)].
- [13] **ATLAS Collaboration** Collaboration, G. Aad et al., *Fiducial and differential cross sections of Higgs boson production measured in the four-lepton decay channel in pp collisions at $\sqrt{s}=8$ TeV with the ATLAS detector*, *Phys.Lett.* **B738** (2014) 234–253, [[arXiv:1408.3226](#)].
- [14] S. Frixione and B. R. Webber, *Matching NLO QCD computations and parton shower simulations*, *JHEP* **0206** (2002) 029, [[hep-ph/0204244](#)].
- [15] P. Nason, *A New method for combining NLO QCD with shower Monte Carlo algorithms*, *JHEP* **0411** (2004) 040, [[hep-ph/0409146](#)].
- [16] S. Frixione, P. Nason, and C. Oleari, *Matching NLO QCD computations with Parton Shower simulations: the POWHEG method*, *JHEP* **0711** (2007) 070, [[arXiv:0709.2092](#)].
- [17] K. Hamilton, P. Nason, E. Re, and G. Zanderighi, *NNLOPS simulation of Higgs boson production*, *JHEP* **1310** (2013) 222, [[arXiv:1309.0017](#)].
- [18] S. Hoche, Y. Li, and S. Prestel, *Higgs-boson production through gluon fusion at NNLO QCD with parton showers*, *Phys.Rev.* **D90** (2014), no. 5 054011, [[arXiv:1407.3773](#)].
- [19] S. Hoeche, Y. Li, and S. Prestel, *Drell-Yan lepton pair production at NNLO QCD with parton showers*, [[arXiv:1405.3607](#)].
- [20] A. Karlberg, E. Re, and G. Zanderighi, *NNLOPS accurate Drell-Yan production*, *JHEP* **1409** (2014) 134, [[arXiv:1407.2940](#)].
- [21] K. Hamilton, P. Nason, C. Oleari, and G. Zanderighi, *Merging $H/W/Z + 0$ and 1 jet at NLO with no merging scale: a path to parton shower + NNLO matching*, *JHEP* **1305** (2013) 082, [[arXiv:1212.4504](#)].
- [22] D. Graudenz, M. Spira, and P. Zerwas, *QCD corrections to Higgs boson production at proton proton colliders*, *Phys.Rev.Lett.* **70** (1993) 1372–1375.
- [23] M. Spira, A. Djouadi, D. Graudenz, and P. Zerwas, *Higgs boson production at the LHC*, *Nucl.Phys.* **B453** (1995) 17–82, [[hep-ph/9504378](#)].
- [24] R. Harlander and P. Kant, *Higgs production and decay: Analytic results at next-to-leading order QCD*, *JHEP* **0512** (2005) 015, [[hep-ph/0509189](#)].
- [25] C. Anastasiou, S. Beerli, S. Bucherer, A. Daleo, and Z. Kunszt, *Two-loop amplitudes and master integrals for the production of a Higgs boson via a massive quark and a scalar-quark loop*, *JHEP* **0701** (2007) 082, [[hep-ph/0611236](#)].
- [26] U. Aglietti, R. Bonciani, G. Degrossi, and A. Vicini, *Analytic Results for Virtual QCD Corrections to Higgs Production and Decay*, *JHEP* **0701** (2007) 021, [[hep-ph/0611266](#)].

- [27] R. Bonciani, G. Degrossi, and A. Vicini, *Scalar particle contribution to Higgs production via gluon fusion at NLO*, *JHEP* **0711** (2007) 095, [[arXiv:0709.4227](#)].
- [28] R. K. Ellis, I. Hinchliffe, M. Soldate, and J. van der Bij, *Higgs Decay to tau+ tau-: A Possible Signature of Intermediate Mass Higgs Bosons at the SSC*, *Nucl.Phys.* **B297** (1988) 221.
- [29] U. Baur and E. N. Glover, *Higgs Boson Production at Large Transverse Momentum in Hadronic Collisions*, *Nucl.Phys.* **B339** (1990) 38–66.
- [30] R. V. Harlander, T. Neumann, K. J. Ozeren, and M. Wiesemann, *Top-mass effects in differential Higgs production through gluon fusion at order α_s^4* , *JHEP* **1208** (2012) 139, [[arXiv:1206.0157](#)].
- [31] *MCFM – Monte Carlo for FeMtobarn processes*: <http://mcfm.fnal.gov>, .
- [32] C. Anastasiou, K. Melnikov, and F. Petriello, *Fully differential Higgs boson production and the di-photon signal through next-to-next-to-leading order*, *Nucl.Phys.* **B724** (2005) 197–246, [[hep-ph/0501130](#)].
- [33] C. Anastasiou, S. Bucherer, and Z. Kunszt, *HPro: A NLO Monte-Carlo for Higgs production via gluon fusion with finite heavy quark masses*, *JHEP* **0910** (2009) 068, [[arXiv:0907.2362](#)].
- [34] R. V. Harlander, S. Liebler, and H. Mantler, *SusHi: A program for the calculation of Higgs production in gluon fusion and bottom-quark annihilation in the Standard Model and the MSSM*, *Computer Physics Communications* **184** (2013) 1605–1617, [[arXiv:1212.3249](#)].
- [35] E. Bagnaschi, G. Degrossi, P. Slavich, and A. Vicini, *Higgs production via gluon fusion in the POWHEG approach in the SM and in the MSSM*, *JHEP* **1202** (2012) 088, [[arXiv:1111.2854](#)].
- [36] M. Buschmann, D. Goncalves, S. Kuttimalai, M. Schonherr, F. Krauss, et al., *Mass Effects in the Higgs-Gluon Coupling: Boosted vs Off-Shell Production*, [arXiv:1410.5806](#).
- [37] H. Mantler and M. Wiesemann, *Top- and bottom-mass effects in hadronic Higgs production at small transverse momenta through LO+NLL*, *Eur.Phys.J.* **C73** (2013), no. 6 2467, [[arXiv:1210.8263](#)].
- [38] R. V. Harlander, H. Mantler, and M. Wiesemann, *Transverse momentum resummation for Higgs production via gluon fusion in the MSSM*, *JHEP* **1411** (2014) 116, [[arXiv:1409.0531](#)].
- [39] M. Grazzini and H. Sargsyan, *Heavy-quark mass effects in Higgs boson production at the LHC*, *JHEP* **1309** (2013) 129, [[arXiv:1306.4581](#)].
- [40] A. Banfi, P. F. Monni, and G. Zanderighi, *Quark masses in Higgs production with a jet veto*, *JHEP* **1401** (2014) 097, [[arXiv:1308.4634](#)].
- [41] J. M. Campbell, R. K. Ellis, R. Frederix, P. Nason, C. Oleari, et al., *NLO Higgs Boson Production Plus One and Two Jets Using the POWHEG BOX, MadGraph4 and MCFM*, *JHEP* **1207** (2012) 092, [[arXiv:1202.5475](#)].
- [42] K. Hamilton, P. Nason, and G. Zanderighi, *MINLO: Multi-Scale Improved NLO*, *JHEP* **1210** (2012) 155, [[arXiv:1206.3572](#)].
- [43] S. Catani, F. Krauss, R. Kuhn, and B. Webber, *QCD matrix elements + parton showers*, *JHEP* **0111** (2001) 063, [[hep-ph/0109231](#)].
- [44] G. Altarelli and G. Parisi, *Asymptotic Freedom in Parton Language*, *Nucl.Phys.* **B126** (1977) 298.

- [45] A. Martin, W. Stirling, R. Thorne, and G. Watt, *Parton distributions for the LHC*, *Eur.Phys.J.* **C63** (2009) 189–285, [[arXiv:0901.0002](#)].
- [46] A. Banfi, P. F. Monni, G. P. Salam, and G. Zanderighi, *Higgs and Z-boson production with a jet veto*, *Phys.Rev.Lett.* **109** (2012) 202001, [[arXiv:1206.4998](#)].